arXiv:cond-mat/9911258v1 [cond-mat.str-el] 17 Nov 1999

Optical Absorption of CuO_3 antiferromagnetic chains at finite temperatures

Eduardo Gagliano, Fabian Lema, Silvia Bacci, Juan José Vicente
Comisión Nacional de Energía Atómica, Centro Atómico Bariloche and Instituto Balseiro, 8400 S.C. de Bariloche (RN), Argentina.

J. Lorenzana*
Istituto Nazionale di Fisica della Materia - Dipartimento di Fisica, Università di Roma "La Sapienza", Piazzale A. Moro 2, I-00185 Roma
(February 1, 2008)

We use a high-statistic quantum Monte Carlo and Maximum Entropy regularization method to compute the dynamical energy correlation function (DECF) of the one-dimensional (1D) $S = 1/2$ antiferromagnetic Heisenberg model at finite temperatures. We also present a finite temperature analytical ansatz for the DECF which is in very good agreement with the numerical data in all the considered temperature range. From these results, and from a finite temperature generalisation of the mechanism proposed by Lorenzana and Sawatsky [Phys. Rev. Lett. **74**, 1867 (1995)], we compute the line shape for the optical absorption spectra of multimagnon excitations assisted by phonons for quasi 1D compounds. The line shape has two contributions analogous to the Stokes and anti-Stokes process of Raman scattering. Our low temperature data is in good agreement with optical absorption experiments of CuO_3 chains in Sr_2CuO_3. Our finite temperature results provide a non trivial prediction on the dynamics of the Heisenberg model at finite temperatures that is easy to verify experimentally.

78.30.Hv,75.40.Gb,75.50.Ee,74.72.-h

I. INTRODUCTION

Infrared optical absorption measurements[1] on charge-transfer insulators such as Sr_2CuO_3 and the isostructural compound Ca_2CuO_3 have shown that these experiments provide important insights in our understanding of the spin dynamics of the underlying CuO_3 chains. The observed bands are analogous to the bands found in cuprates with CuO planes[2–5] at mid infrared energies.

Although direct absorption of magnetic excitations is not possible in the usual optical transitions induced by dipole interaction, they are allowed by the assistance of phonons[6–9] whose effect is to effectively lower the symmetry of the lattice giving rise to a finite dipole moment[10]. This effective dipole moment for processes involving one phonon and spin excitations has been obtained perturbatively starting from the three-band Hubbard model in the presence of slowly varying electric and phonon fields (see Ref. 6,7 hereafter LS) or using exact diagonalization of small clusters[11].

An effective low-energy description of the spin degrees of freedom of the CuO_3 chain is given by the one-dimensional (1D) $S = 1/2$ antiferromagnetic Heisenberg Hamiltonian (AFH).

$$H_{\rm mag} = J \sum_i \boldsymbol{S}_i \boldsymbol{S}_{i+1}. \quad (1)$$

Although the energy spectrum of this many-body quantum problem has been solved a long time ago[12], the computation of its dynamical properties remains a challenge. So far most of the numerical results on dynamical properties come from exact diagonalization of small systems, and more recently from quantum Monte Carlo (QMC) simulations combined with the Maximum Entropy (MaxEnt) analytic continuation procedure of noisy data. This combination has been used to calculate the dynamical spin correlation function of the 1D[13,14] and 2D[15,16] Heisenberg model and correctly describes the inelastic neutron scattering of $CuCl_2.2N(C_5H_5)$[13] and La_2CuO_4[15,16].

The estimated intrachain exchange energy of Sr_2CuO_3 is $J \sim 0.26eV$[1,8,17]. For an electric field parallel to the CuO_3 chain the absorption band at low temperatures ($T = 32K$) is wide, starts at the relevant phonon frequency ($\omega_0 = 0.07$eV), extends up to $\omega = \omega_0 + \pi J \sim 0.9$eV (the maximum energy of two spinons dispersion) and has a singularity at $\omega = \omega_0 + \pi J/2 \sim 0.48$eV (the maximum of the des Cloizeaux-Pearson dispersion). For an electric field perpendicular to the chain axis, the spectrum is weak and structureless. This kind of response is typical of 1D systems.

Experimental features[1] of the optical absorption spectrum $\alpha(\omega)$ of these materials may be analysed applying LS idea of phonon-assisted multimagnon optical absorption with a $T = 0$ analytical ansatz for the dynamical energy correlation function (DECF)[8]. Numerical studies show that at $T = 0$ the dynamical structure factor and the DECF of the AFH model have a significant structure in the $\omega - q$ plane between $\omega_1(q) = \pi J|\sin(q)|/2$ (the des Cloizeaux-Pearson dispersion relation) and $\omega_2(q) = \pi J|\sin(q)|$, the maximum of the two-spinon continuum. At zero temperature the LS mechanism gives structure at the energy of the relevant phonon plus the energy of the magnetic excitations and the computed spectrum is in excellent agreement with the experimental one[8] at low temperatures.

Here we present numerical results for the *finite temperature* DECF. For systems up to $N_s = 32$, we perform

a high-statistic quantum Monte Carlo simulation and obtain the spectrum by the MaxEnt analytic continuation regularization technique of noisy data. The Monte Carlo technique is a non-perturbative approach and so useful to check the validity of the different approximations involved on the analytical results; the considered system sizes are large enough to safely extrapolate to the thermodynamic limit. The technique is presented on Sec. III.

One of our goals is to study finite temperature effects on the optical absorption spectra. Although the temperature dependence of the spectra has been studied experimentally in 2D compounds[4,5] to the best of our knowledge no 1D studies have been reported yet. In Sec. II we discuss LS theory at finite temperatures.

We also check the validity of the $T = 0$ ansatz[8] for the DECF and, based on bosonization results[18], we generalise this ansatz to finite temperatures (Sec. IV). The analytical ansatz is in very good agreement with the numerical data in all the considered temperature range. Finally, our results for the optical absorption spectra (Sec. V) are in excellent agreement with available low temperature experimental (Ref. 8) data and provide a prediction on the finite temperature dynamics of a 1D Heisenberg system that can be tested experimentally.

II. PHONON-ASSISTED IR ABSORPTION OF MAGNONS AT FINITE TEMPERATURES

A. Model

In this section we generalise the $T = 0$ theory of LS to finite temperatures. We consider an effective Hamiltonian describing the coupling of light with one-phonon-multimagnon excitations: $H = H_0 + H_1$, where $H_1 = -PE$, P (E) is the magnitude of the dipole moment operator (electric field) in the chain direction. The unperturbed Hamiltonian is:

$$H_0 = H_{\rm mag} + H_{\rm ph}. \tag{2}$$

here the magnetic part is the Heisenberg model Eq. (1) and for the phonon Hamiltonian we take a single branch: the Cu-O stretching mode in the chain direction[6]

$$H_{\rm ph} = \sum_q \omega_q (a_q^\dagger a_q + \frac{1}{2}) \tag{3}$$

where ω_q is the phonon frequency. The dipole moment is

$$P = \sum_q \lambda_q A_q B_{-q.} \tag{4}$$

where $A_q = (a_q + a_{-q}^\dagger)$, B_q is the Fourier transform of $B_i \equiv \boldsymbol{S}_i \boldsymbol{S}_{i+1}$. The strength of the coupling of light with these excitations is given by:

$$\lambda_k = 4 q_{\rm A} \sqrt{\frac{\hbar}{2M\omega_k}} \sin^2(\frac{k}{2}) \tag{5}$$

here M is the oxygen mass and $q_{\rm A}$ a material dependent effective charge which is in the range $0.1 \sim 0.4e$[6–8].

In the definition of the dipole moment operator we have neglected terms like conventional phonon absorption ($P = \lambda' A_0$) which are outside the scope of this work.

B. Optical absorption

From general considerations the optical absorption spectrum is given by

$$\alpha(\omega) = \frac{2\omega}{c} {\rm Im}(\sqrt{\epsilon(\omega)}) \tag{6}$$

where $\epsilon = \epsilon_1(\omega) + i\epsilon_2(\omega)$ is the complex-dielectric function and c is the speed of light. Assuming weak absorption, $\epsilon_1 >> \epsilon_2$, Eq. (6) can be rewritten as,

$$\alpha(\omega) = \frac{4\pi}{c\sqrt{\epsilon_1}} \sigma(\omega) \tag{7}$$

where $\sigma(\omega)$ is the frequency dependent conductivity which can be written in terms of the Fourier transform of the real time dipole-dipole retarded Green function. Using the Lehman representation and the fluctuation-dissipation theorem one can write for the real part,

$$\sigma = \frac{\pi\omega(1-e^{-\beta\omega})}{ZV} \sum_{N,M} e^{-\beta\varepsilon_N} |\langle N|P|M\rangle|^2 \delta(\omega + \varepsilon_N - \varepsilon_M) \tag{8}$$

here $H_0|M\rangle = \varepsilon_M|M\rangle$, Z is the partition function, β the inverse temperature and V the volume. In Eq. (2) weak magnon-phonon interactions were assumed, i.e in the absence of electric fields any term coupling magnons with phonons was neglected. Under this assumption the eigenstates of the system are products of phonon states times magnetic states,

$$|M\rangle = |m\rangle|\mu\rangle \tag{9}$$

where $|\mu\rangle$ ($|m\rangle$) labels an eigenstate of $H_{\rm mag}$ ($H_{\rm ph}$) with energy E_μ (ω_m). (From now on we use μ, ν to label magnetic eigenstates and m, n for phonon eigenstates.)

The optical conductivity can be written as:

$$\sigma = \frac{\pi\omega(1-e^{-\beta\omega})}{V Z_{\rm mag} Z_{\rm ph}} \sum_{qmn\mu\nu} e^{-\beta(\omega_n + E_\nu)} \lambda_q^2 \times \tag{10}$$
$$|\langle n|A_q|m\rangle|^2 |\langle \mu|B_q|\nu\rangle|^2 \delta(\omega + \omega_n - \omega_m + E_\nu - E_\mu)$$

where $Z_{\rm ph} = \sum_n e^{-\beta\omega_n}$ and $Z_{\rm mag} = \sum_\nu e^{-\beta E_\nu}$. Using the fact that A_q creates or destroys a phonon of momentum q, we can evaluate the phonon part and we get for the optical conductivity,

$$\sigma = \frac{\pi\omega(1-e^{-\beta\omega})}{V} \times \sum_q \lambda_q^2[(1+n_q)J_q(\omega-\omega_q) + n_q J_q(\omega+\omega_q)] \quad (11)$$

n_q is the Bose occupation number for q-momentum phonons. All the magnetic information is stored in the function,

$$J_q(\omega) = \frac{1}{Z_{\rm mag}} \sum_{\mu\nu} e^{-\beta E_\nu} |\langle\mu|B_q|\nu\rangle|^2 \delta(\omega + E_\nu - E_\mu) \quad (12)$$

The first term in the brackets in Eq. (11) corresponds to process in which the incoming photon creates a magnetic excitation and a phonon; the second term corresponds to the destruction of a phonon from the bath with creation of a magnetic excitation. The first term does not vanish at zero temperature and it is the one considered by LS. It gives structure at the energy of the phonons plus the energy of the magnetic excitations. The last term is new, vanish at zero temperature and gives structure at the energy of the magnetic excitation minus the energy of the phonon. Notice the similarity with the Stokes and anti-Stokes processes in Raman scattering.

J_q can be evaluated from the retarded Green function using the fluctuation-dissipation theorem:

$$J_q(\omega) = \frac{-\,{\rm Im}\, G_q(\omega)}{\pi(1-e^{-\beta\omega})}. \quad (13)$$

where $G_q(\omega)$ is the Fourier transform of the real time retarded Green function

$$G_q(t) = -i\theta(t) < [B(q,t), B(-q,0)] > . \quad (14)$$

We also define

$$\Lambda_q(\omega) \equiv (1-e^{-\beta\omega}) J_q(\omega) = -\frac{1}{\pi}\,{\rm Im}\, G_q(\omega) \quad (15)$$

which is an odd function of ω and is evaluated in the next section using MaxEnt and in Sec. IV using an analytical ansatz.

III. QUANTUM MONTE CARLO AND MAXIMUM-ENTROPY ANALYTIC CONTINUATION

In order to compute the magnetic response we perform a World Line quantum Monte Carlo simulation.[19] The algorithm is based on a path integral approach. To evaluate the average of physical observables,

$$\langle O\rangle = \frac{{\rm tr}(Oe^{-\beta H_{\rm mag}})}{Z_{\rm mag}},$$

the method divides the $0 < \tau < \beta$ interval into L parts, each one of width $\Delta\tau = \beta/L$ and breaks the 1D Hamiltonian $H_{\rm mag}$ in two commuting parts H_1 and H_2, each one corresponding to a different sublattice, even and odd respectively. Introducing at each one of the 2L intermediate times a complete set of S_z eigenstates and using the Suzuki-Trotter formula[20]

$$e^{-\Delta\tau H_{\rm mag}} = e^{-\Delta\tau H_1} e^{-\Delta\tau H_2}[1 + O(\Delta\tau^2)],$$

one can evaluate the resulting matrix elements and insure, making $\Delta\tau \to 0$, that the error introduced by the Suzuki-Trotter approximation is smaller than the statistical error. The updating procedure has two different kinds of moves: local changes conserve the total spin projection S_z and global moves allow magnetisation fluctuations.[21]

We implemented a multispin code. This allows an efficient integer algebra manipulation of one-bit spins packed into 32-bits words and achieves a high speed. For different values of $\beta = 1, 5, 10$ (in units of J) we fix $\Delta\tau = 0.125$; given this value of $\Delta\tau$ the acceptance rates of local and global moves are always less than 10%, this is fixed by the algorithm and can not be changed. For $\beta = 10$ we performed ~ 100 independent runs, 10^6 iterations each, measuring every 1000. It was necessary to evaluate the spin autocorrelation function in order to insure that measurements were not correlated.

Quantum Monte Carlo simulations allow us to compute imaginary-time τ correlation functions. Besides the DECF results presented in this work, as a check of our code, we have also computed static properties, the spin dynamic structure factor and for small systems, up to $N_s = 16$ sites, tested against exact diagonalization[22] obtaining the optical absorption spectra from the spectral representation of the DECF. All the results shown here correspond to a system of size $N_s = 32$. For low temperatures, $\beta = 10$ and $N_s = 32$ we monitored $\langle E\rangle^2 \sim \langle E^2\rangle = \frac{1}{N_s}\sum_{l=0,\ldots,N_s-1} < B_i B_{i+l} >$: in all cases the differences were less than 5×10^{-4}.

The imaginary time energy correlation function is periodic in τ with period β and is given by

$$G_q(\tau) = \langle B_q(\tau) B_{-q}(0)\rangle \quad (16)$$

where $B_q(\tau) = e^{\tau H} B_q e^{-\tau H}$ and $0 < \tau < \beta$.

For the analytic continuation problem of calculating the spectral density $\Lambda_q(\omega)$ associated with the imaginary-time Green's function $G_q(\tau)$ one has to invert the integral equation,

$$G_q(\tau) = \int_{-\infty}^{+\infty} d\omega K(\tau,\omega)\Lambda_q(\omega) \quad (17)$$

where K is the Kernel for bosons

$$K(\tau,\omega) = \frac{e^{-\tau\omega}}{1-e^{-\beta\omega}} \quad (18)$$

It is well known that Fredholm integral equations of the first kind are classical examples of ill-posed problems. After discretization of the frequency interval one ends up

with a discrete ill-posed problem. Because QMC simulations provide a noisy and incomplete set of data $\bar{G}_q(\tau_n)$, $\tau_n = n\Delta\tau$ the direct inversion is ill-conditioned and the $\Lambda_q(\omega)$ spectrum cannot be uniquely determined. Here the bar over $G_q(\tau_n)$ indicates a Monte Carlo average as explained below.

The MaxEnt approach is a regularization method for this kind of ill-posed problems which provides *an unique solution* compatible with Bayesian statistic and prior knowledge.[23] The best image compatible with the data is obtained maximising

$$Q = \lambda S - \frac{1}{2}\chi^2$$

by solving $\nabla Q = 0$. Here λ is a regularization parameter and χ^2 the misfit statistic which not only includes the statistical errors of the data but also the correlations between different imaginary-time data points. The misfit statistic is given by

$$\chi^2 = \sum_{i,j}[G_q(\tau_i) - \bar{G}_q(\tau_i)]C_{ij}^{-1}[G_q(\tau_j) - \bar{G}_q(\tau_j)] \qquad (19)$$

where C is the covariance matrix that takes into account the imaginary-time correlation of the data. S is the Shannon-Jaynes entropy of the spectrum defined with respect to the initial guess model $m(\omega)$:

$$S = -\int_{-\infty}^{+\infty} d\omega[\Lambda_q(\omega) - m(\omega) - \Lambda_q(\omega)ln(\Lambda_q(\omega)/m(\omega))] \qquad (20)$$

$m(\omega)$ is the best guess in absence of prior knowledge on the spectrum. We took a flat model.

In practice, functional maximisation is reduced to search in a multidimensional parameter space by a Simpson evaluation of the integrals. We performed a variable ω-discretization with 100-200 frequency points.[24]

We binned the data G_q until we obtained a Gaussian distribution that satisfies several criteria, Kolmogorov-Smirnov, skewness, Kurtosis and standard deviation.[25] Fig. 1 presents an example: starting from $\sim$ 100000 QMC-data the four gaussianity tests are satisfied grouping the data on $100 - 1000$ bins, each one an average of $1000 - 100$ QMC-data respectively. We consider $N = 1000$ bins. After this binning the imaginary time Monte Carlo averages $\bar{G}_q$ have relative errors less than 10^{-3}.

A zero temperature sum rule[8] was used to check the low temperature data and was found to be satisfied within a 2% error.

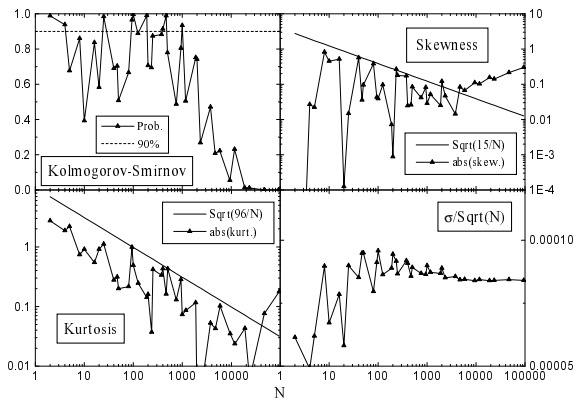

FIG. 1. The 4 different gaussianity tests that we performed on our data. The independent variable is N the number of bins. For Kolmogorov-Smirnov we plot the probability of the data being Gaussian. We can see that up to $N = 1000$ bins there is a high probability of the data being Gaussian. For Skewness and Kurtosis crossing over the full line indicates departure from Gaussianity. From the standard deviation (σ) test we can see that under $N = 100$ bins the data does not behave as Gaussian.

IV. ANSATZ FOR THE DYNAMIC ENERGY CORRELATION FUNCTION AT FINITE TEMPERATURES

We present here a finite temperatures generalisation of the $T = 0$ ansatz (Ref. 8), which agrees very well with the numerical results.

The $T = 0$ ansatz can be written in terms of $G_q^{XY'}(\omega)$, the retarded Green function of the XY model,

$$-\frac{1}{\pi}\,\mathrm{Im}\,G_q^{XY'}(\omega) = \frac{\theta[\omega - \omega_1(q)]\theta[\omega_2(q) - \omega]\sqrt{\omega_2^2(q) - \omega^2}}{\omega_2^2(q)} \qquad (21)$$

here the prime indicates that the energy scale has been changed according to $J_{XY} \to J\pi/2$. With this notation the zero temperature ansatz reads

$$\mathrm{Im}\,G_q(\omega) = \mathrm{Im}\,G_q^{XY'}(\omega)[A\sqrt{Jf_\pi(\omega)} + BJf_q(\omega)] \qquad (22)$$

where A and B are constants of values A= 2.4, B= 0.6 and we defined

$$f_q(\omega) = \frac{1}{\sqrt{\omega^2 - \omega_1^2(q)}}. \quad (23)$$

The term $1/\sqrt{\omega^2 - \omega_1^2(q)}$ in Eqs. (22),(23) is chosen to reproduce the behaviour of bosonization at low energies. For details see Ref. 8.

To generalise this ansatz to finite temperatures we simply replace $G_q^{XY'}(\omega)$ and $f_q(\omega)$ by their finite temperature versions. At finite temperature it is trivial to compute $G_q^{XY'}(\omega)$ by mapping the XY model to a free Fermion model[26],

$$\mathrm{Im}\, G_q^{XY'}(\omega) = -\frac{\sinh(\frac{\beta\omega}{2})\,\mathrm{Re}\,\sqrt{\omega_2^2(q) - \omega^2}}{\omega_2^2(q)\left[\cosh(\frac{\beta\omega}{2}) + \cosh(\frac{\beta\sqrt{\omega_2^2(q)-\omega^2}}{2\tan(\frac{q}{2})})\right]} \quad (24)$$

On the other hand the low energy behaviour predicted by bosonization becomes[18]:

$$f_q(\omega) = -2\,\mathrm{Im}(\beta I_1[\beta\frac{\omega - \omega_2(q)}{2\pi}] I_1[\beta\frac{\omega + \omega_2(q)}{2\pi}]) \quad (25)$$

where we have defined

$$I_1(y) = \frac{1}{\sqrt{8\pi}}\frac{\Gamma(\frac{1}{4} + \frac{1}{2}iy)}{\Gamma(\frac{3}{4} + \frac{1}{2}iy)} \quad (26)$$

Eqs. (22),(24)-(26) define our finite temperature ansatz. The spectral density Λ is computed from the Green function through expression Eq. (15).

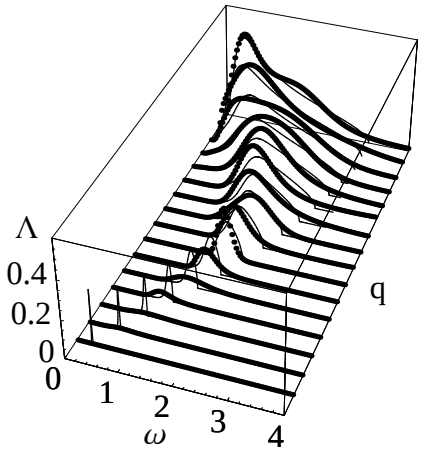

FIG. 2. The spectral density Λ as a function of q and ω for $\beta = 10$ ($J = 1$). The dots are the MaxEnt data for $N_s = 32$ and the lines the finite temperature analytic ansatz.

In Fig. 2 we compare the finite temperature ansatz with the Maximum Entropy data for different momenta and temperatures. We see that both approaches give quite similar results. In particular the width of the peak close to $q = \pi$ agrees remarkably well (See Fig. 3).

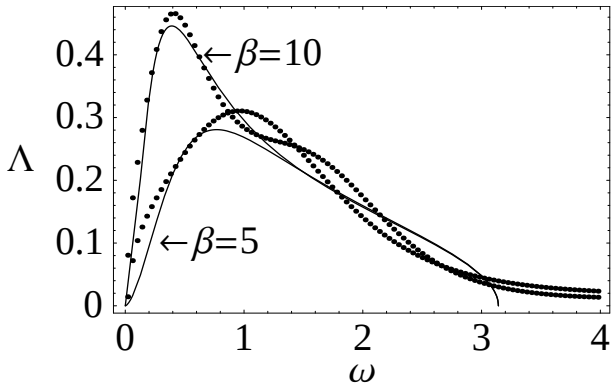

FIG. 3. Λ as function of ω for $q = \pi$ and $\beta = 5, 10$ ($J = 1$). Dots and lines as in Fig. 2.

For $q \sim 0$ the ansatz gives a much narrower peak than the MaxEnt data, however this disagreement is of no importance for our purpose since this part of the spectrum gives a negligible contribution to the IR line shape.

V. INFRARED ABSORPTION SPECTRA

The optical spectra for phonon-assisted multimagnon absorption is given by Eqs. (7),(11). For the materials under consideration the momentum dependence of the phonons can be neglected and we can take Einstein phonons: $\omega_q \equiv \omega_0$, $n_q \equiv n_0$. In this case it is useful to define the following function,

$$I(\omega) = -\frac{8}{N_s\pi}\sum_q \sin^4(q/2)\,\mathrm{Im}\, G_q(\omega), \quad (27)$$

In Fig. 4 we show this function for different values of the inverse temperature. From this figure the absorption coefficient for other materials can be computed without the cumbersome integration of the ansatz. The absorption coefficient for a specific material is,

$$\alpha = \alpha_0\omega(1 - e^{-\beta\omega})[\frac{(1+n_0)I(\omega - \omega_0)}{1 - e^{-\beta(\omega-\omega_0)}} + \frac{n_0 I(\omega + \omega_0)}{1 - e^{-\beta(\omega+\omega_0)}}] \quad (28)$$

where

$$\alpha_0 = \frac{4N_s\pi^2 q_A^2}{c\sqrt{\epsilon_1}MV\omega_0}.$$

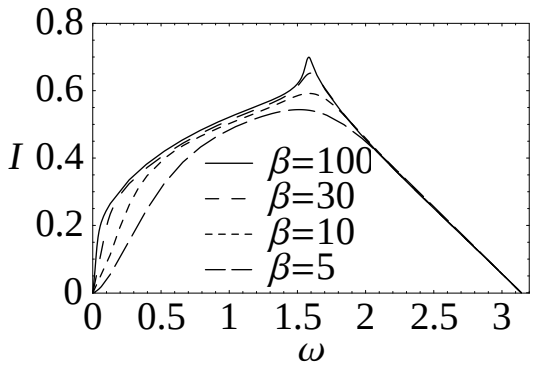

FIG. 4. $I(\omega)$ for different values of β in units such that $J = 1$.

In Fig. 5 we show our results for the midinfrared absorption spectra obtained from the analytical ansatz and compare with experimental measurements on Sr_2CuO_3 at $T = 32K$. As a check we can see that our low temperature results are in excellent agreement with experimental data.

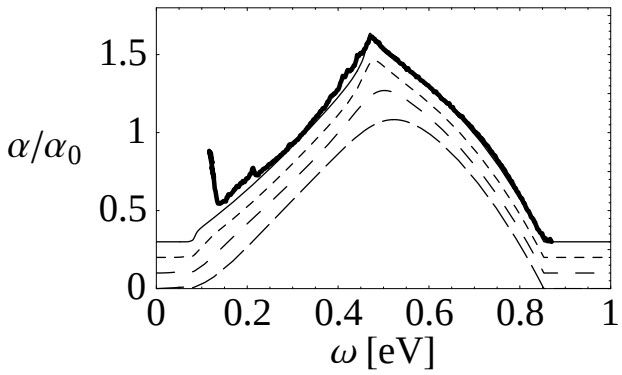

FIG. 5. We show α as a function of ω for Sr_2CuO_3 ($J = 0.246$eV, $\omega_0 = 0.08$eV) for (from bottom to top) $\beta/J = 5, 10, 30, 100$, using the finite temperature ansatz. The curves are shifted by 0.1 for clarity. The thick line is the experimental data after Ref. 1

VI. SUMMARY AND DISCUSSION

We have used quantum Monte Carlo and MaxEnt methods to calculate the dynamical energy correlation function, $\Lambda_q(\omega)$, for S= 1/2 antiferromagnetic Heisenberg chains at finite temperatures.

Based on bosonization at finite temperatures we also present a finite temperature ansatz for the spectral density of the DECF which is in very good agreement with numerical data in all the temperature range. Since these two approaches are independent the agreement gives us confidence on the accuracy of both results. In particular for $q = \pi$, the agreement of the width of the spectral function is a quite strong test for the numerical data of finite systems because in the ansatz that width is completely determined by bosonization (which is an asintotically exact approach).

From the ansatz we obtain the optical absorption which, at low temperatures, is in excellent agreement with available CuO_3 measurements. This is expected since the finite temperature ansatz converges to the zero temperature ansatz as the temperature is lowered and for the latter good agreement has already been found[8].

Naively one can expect that finite temperature effects will affect the line shape at energies smaller than the temperature. As Fig. 5 show this expectation is wrong. Dramatic changes occur close to the singularity at energy $\omega_0 + \pi J/2$. This can be understood by considering the mapping of the problem to a half-filed interacting-fermion band[26]. The particle hole transitions that have the required energy to contribute to the singularity are excitations of fermions from just below the Fermi level to the top of the band and particle hole transitions from the bottom of the band to just above the Fermi level. Since both process involve the fermions at the Fermi level they get strongly affected by the smoothing of the Fermi distribution function around the Fermi energy. This explains the rounding of the singularity with temperature. Of course the low energy part of the spectrum also involves excitations close to the Fermi level and gets affected as can be seen from Fig. 4.

Our finite temperature line shape is a non trivial prediction on the dynamics of the 1D Heisenberg model at finite temperatures. We hope that this result will stimulate further experimental work in this direction.

VII. ACKNOWLEDGEMENTS

All of us are supported by the Consejo Nacional de Investigaciones Científicas y Técnicas, Argentina. Partial support from Fundación Antorchas under grant 13016/1, from Agencia Nacional de Promoción Científica y Tecnológica under grant PMT-PICT0005 and PICT 03-00121-02153 and CONICET grant 4952/96 and INFM PRA (HTSC) are gratefully acknowledged. J. L. thanks the IRS group (Rome) for hospitality.

* Permanent Address: Centro Atómico Bariloche (CONICET) and Instituto Balseiro, 8400 S. C. de Bariloche, Argentina.

[1] H.Suuzura, H.Yasuhara, A. Furusaki, N. Nagaosa and Y. Tokura.Phys. Rev. Lett. **76**, 2579 (1996).
[2] J.D. Perkins *et al.*, Phys. Rev. Lett. **71**, 1621 (1993).
[3] J.D. Perkins, Ph.D. thesis, Massachusetts Institute of Technology, Cambridge, Massachusetts, 1994.
[4] J.D. Perkins, *et al.*, Phys. Rev. B. **58**, 9390 (1998).
[5] H. S. Choi, E.J. Choi and Y. J. Kim, Physica C, **304** 66, (1998).
[6] J. Lorenzana and G. A. Sawatzky, Phys. Rev. Lett. **74**,1867 (1995).
[7] J. Lorenzana and G. A. Sawatzky, Phys. Rev. B **52**, 9576 (1995).
[8] J. Lorenzana and R. Eder, Phys. Rev. B **55**, R3358 (1997).
[9] J. Lorenzana, J. Eroles and S. Sorella, Phys. Rev. Lett. (in press).
[10] Y. Mitzuno and S. Koide, Phys. Kondens. Materie **2**, 179 (1964)
[11] D. Garcia, J. Eroles and J. Lorenzana, Phys. Rev. B. **58** 13574 (1998).
[12] H. Bethe, Z. Phys. **71** 205 (1931).
[13] J. Deisz, M. Jarrell and D.L. Cox, Phys. Rev. B **42** 4869, (1990).
[14] O. A. Starykh, A. W. Sandvik and R. R. Singh, Phys. Rev. B **55**, 14953 (1997).
[15] M. Makivic and M. Jarrell, Phys. Rev. Lett. **68**, 1770 (1992).
[16] M. Greven *et al.*, Phys. Rev. Lett. **72**, 1096 (1994).
[17] T. Ami *et al.* Phys. Rev. B.**51**, 5994 (1995).
[18] M.C. Cross and D.S. Fisher, Phys. Rev. B **19**, 402 (1979).
[19] J.E. Hirsch, R.L. Sugar, D.J. Scalapino and R. Blankenbecler, Phys. Rev. B **26**, 5033 (1982).
[20] M. Suzuki, Prog. Theor. Phys. **56** 1457, (1976).
[21] M. Marcu, in *Quantum Monte Carlo Methods in Equilibrium and Non-Equilibrium Systems*. ed. by M. Suzuki (Springer, Berlin, 1987).
[22] E. Gagliano and S. Bacci, Phys. Rev. B **42**, 8772 (1990).
[23] *MaxEnt and Bayesian Methods*, ed. by J. Skilling (Kluwer Academic Dordrecht, 1989); R.N. Silver, D.S. Sivia and J. Gubernatis, Phys. Rev. B **41**, 2380 (1990).
[24] Following Bryan and Skilling, Mon. Not. R. Ast. Soc. **211**, 111 (1984), we conducted an iterative search in the image space by selecting a few independent searching directions with the criteria that the addition of other independent directions do not change the obtained spectrum. We have found that at least 6 directions are needed, in contrast to common practice which uses only 3.
[25] Numerical Recipes, by W.H. Press, S.A. Teukolsky, W.T. Vetterling and B.P. Flannery, Cambridge University Press.
[26] Solýom, Adv. in Phys. **28**, 261 (1979).